

See discussions, stats, and author profiles for this publication at: <https://www.researchgate.net/publication/277783274>

Evaluation of Factors To Determine Platelet Compatibility by Using Self-Assembled Monolayers with a Chemical Gradient

ARTICLE *in* LANGMUIR · JUNE 2015

Impact Factor: 4.46 · DOI: 10.1021/acs.langmuir.5b01216 · Source: PubMed

READS

25

5 AUTHORS, INCLUDING:



Masaru Tanaka

Yamagata University

68 PUBLICATIONS 2,437 CITATIONS

[SEE PROFILE](#)



Tomohiro Hayashi

Tokyo Institute of Technology

74 PUBLICATIONS 1,131 CITATIONS

[SEE PROFILE](#)

Evaluation of Factors To Determine Platelet Compatibility by Using Self-Assembled Monolayers with a Chemical Gradient

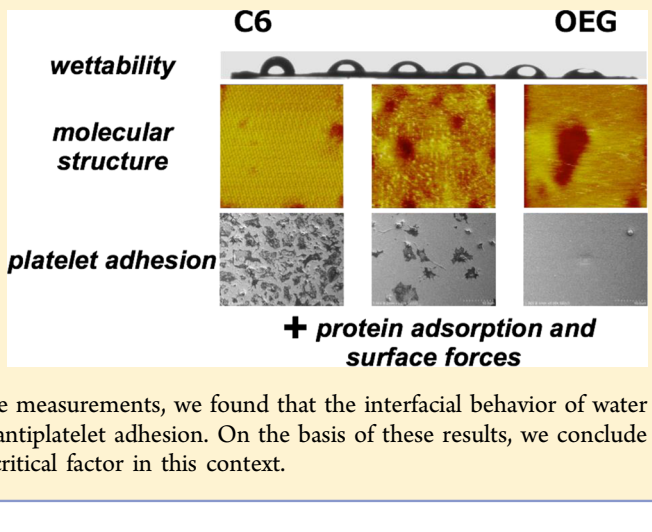
Taito Sekine,[†] Yusaku Tanaka,[†] Chikako Sato,[‡] Masaru Tanaka,^{‡,§} and Tomohiro Hayashi^{*,†}

[†]Department of Electronic Chemistry, Interdisciplinary Graduate School of Science and Engineering, Tokyo Institute of Technology, 4259 Nagatsuta-cho Midori-ku, Yokohama, Kanagawa 226-8502, Japan

[‡]Department of Biochemical Engineering, Graduate School of Science and Engineering, Yamagata University, Jonan 4-3-16, Yonezawa 992-0038, Japan

Supporting Information

ABSTRACT: Intercorrelation among surface chemical composition, packing structure of molecules, water contact angles, amounts and structures of adsorbed proteins, and blood compatibility was systematically investigated with self-assembled monolayers (SAMs) with continuous chemical composition gradients. The SAMs were mixtures of two thiols: *n*-hexanethiol (hydrophobic and protein-adsorbing) and hydroxyl-tri(ethylene glycol)-terminated alkanethiol (hydrophilic and protein-resistant) with continuously changing mixing ratios. From the systematic analyses, we found that protein adsorption is governed both by sizes of proteins and hydrophobic domains of the substrate. Furthermore, we found a clear correlation between adsorption of fibrinogen and adhesion of platelets. Combined with the results of surface force measurements, we found that the interfacial behavior of water molecules is profoundly correlated with protein resistance and antiplatelet adhesion. On the basis of these results, we conclude that the structuring of water at the SAM–water interface is a critical factor in this context.



INTRODUCTION

Fabrications of blood-compatible surfaces, which are highly inert to blood proteins and cells, are in high demand for the coatings of artificial heart and lungs and artificial blood vessels. Thus far, many kinds of blood-compatible polymers have been reported; they are nonionic poly(ethylene glycol) (PEG), poly(2-methoxyethyl acrylate) (PMEA), zwitterionic poly(2-methacryloyloxyethyl phosphorylcholine) (PMPC), poly(sulfobetaine methacrylate) (PSBMA), and poly(carboxybetaine methacrylate) (PCBMA), to name a few.¹ In spite of the large number of reports on blood-compatible materials, the mechanism underlying their inertness to blood cells and proteins remains unclear. As a result, it is rather difficult to set clear directions for the design of new blood-compatible materials (i.e., functional groups, their densities and spatial distributions, flexibility, mobility, etc.).^{2–4}

In general, when a surface is exposed to blood, the surface is hydrated, immediately followed by the adsorption of plasma proteins. After that, platelets adhere onto the adsorbed proteins, using them as an extracellular matrix. Among the proteins, fibrinogen has been considered as a major determinant for the response (adhesion and activation) of platelets. In particular, Tanaka et al. and Sivaraman and Latour recently reported that the conformation of adsorbed fibrinogen (content of the α -helix) affected the activation of the platelets more than the amount of the adsorbed fibrinogen.^{5,6} Besides

these reports, Sivaraman and Latour recently presented a correlation between the amount of unfolded albumin adsorbed on a surface and the activation of platelets.⁷

Various conclusions in the previous reports clearly suggest that it is essentially required to investigate the intercorrelation among chemical properties (density and spatial distribution of functional groups, surface charges, hydration, etc.), protein adsorption, and platelet adhesion. Self-assembled monolayers (SAMs) provide ideal platforms to investigate the interaction between artificial organic surfaces with biomolecules and cells, because of their highly ordered and well-defined structures and the flexibility with which investigators can control the physicochemical properties of the monolayers by employing thiols with different types of terminal groups.^{8–10} In this work, we fabricated the SAMs with a continuous chemical composition gradient by using an exchange reaction of alkanethiols on Au(111) surfaces.¹¹ In particular, we investigated SAMs consisting of tri(ethylene glycol)-terminated alkanethiol [$\text{HS}-(\text{CH}_2)_{11}-(\text{OCH}_2\text{CH}_2)_3-\text{OH}$] (EG3-OH)^{12,13} and *n*-hexanethiol (C6). The EG3-OH and C6-SAMs are typical protein-resistant and protein-adsorbing SAMs, respectively. Therefore, transition from “protein-resistant” to

Received: April 3, 2015

Revised: May 24, 2015

Published: June 2, 2015

"protein-adsorbing" is expected to be observed in the mixed SAM.

Recently, we reported that the (EG3-OH)-SAM exhibited excellent protein resistance and property of antiplatelet adhesion.¹⁴ In addition, we proposed that a physical barrier of interfacial water in the vicinity of an (EG3-OH)-SAMs suppresses denaturation of protein molecules and deters adsorption of proteins and adhesion of platelets.¹⁴ In this work, we aim to investigate correlations among chemical compositions of the thiols, water contact angles, amounts of adsorbed proteins, and densities of adhered platelets systematically by using SAMs with a chemical gradient.¹¹ In addition, we performed surface force analysis using an atomic force microscope (AFM) to elucidate the behavior of water molecules in the vicinity of the mixed SAMs. Combining the above findings, we discuss major factors to determine the adhesion and activation of platelets and parameters that can be used as possible guideposts to improve platelet compatibility of different surfaces.

EXPERIMENTAL SECTION

Fabrication of SAMs. Au(111) substrates were prepared by vacuum deposition of gold onto freshly cleaved mica ($10 \times 10 \times 0.3$ mm³, S&J Trading Inc.) at 620 K under a vacuum pressure of 10^{-5} – 10^{-6} Pa. The substrates were then annealed at 620 K in a vacuum chamber for 2 h. In this work, we used *n*-hexanethiol [$\text{CH}_3-(\text{CH}_2)_5-\text{SH}$, denoted as C6 hereafter] (Sigma-Aldrich Japan, Tokyo) and triethylene glycol mono-11-mercaptoundecyl ether [$\text{OH}-(\text{CH}_2-\text{CH}_2-\text{O})_3-(\text{CH}_2)_{11}-\text{SH}$, denoted as OEG] (ProChimia, Gdansk) to prepare SAMs with a composition gradient. The chemical gradient was fabricated by immersing the C6-SAM (or OEG-SAM) into a solution of OEG (C6) thiol perpendicularly at constant speed. The reaction time for the molecular exchange depends on the position of the substrate, resulting in a continuous chemical composition gradient on the substrate.

The detail of the fabrication is the followings. First, a fresh gold substrate was immersed in ethanol solution containing the first thiol [C6 or OEG thiol (1 mM)] for 24 h to form an initial monolayer. Then, the substrate with the first monolayer is mounted on a linear motion drive system, which immerses the substrate into an ethanol solution containing the second thiol at variable speeds (0.01–1 mm/min). During this process, part of the molecules constituting the initial SAM experiences an exchange reaction with thiol molecules in the solution. Since the total immersion (exchange) time depends on the position on the substrate, a composition gradient is formed on the substrate.

This approach is different from previously reported ones by using stamps,¹⁵ irradiation of electron beams,^{16,17} or laser beam¹⁸ exchange between partially covered SAMs and thiols in solution.¹⁹ We previously demonstrated the application of our approach to fabricate the SAMs with a chemical gradient.¹¹

Characterization of the SAMs. The chemical composition of the substrate was characterized by X-ray photoelectron spectroscopy (XPS) (Theta Probe, Thermo Electron, U.K.). For the X-ray, Al K α radiation (photon energy of 1486.6 eV and spot size of 100 μm) was used. The density of the OEG thiolate at each point on the mixed SAM with respect to that of the pure OEG-SAM (denoted as ρ hereafter) was evaluated from the peak intensity of the $\text{C}_{1s(\text{C}-\text{O})}$ signal (Supporting Information).¹¹ With this condition (spot size of X-ray and accuracy of the positioning), the standard deviation of ρ is smaller than 0.02, which was evaluated by the cycles of transfer of the samples and measurements.

Scanning tunneling microscopy (STM) measurements were performed using a NanoScope IV (Veeco Inc., Santa Barbara, CA) and a commercially available Pt/Ir tip (80:20). All STM images were obtained in air under constant-current mode at room temperature.

The bias voltage and tunneling current were fixed at 500 mV and 300 pA, respectively.

Static water contact angles were measured by the sessile-drop method on a Krüss DSA10 contact-angle meter. They were recorded at 25 ± 0.5 °C with distilled water. All droplets were 0.2 μL in volume ($n = 3$).

Protein Adsorption Tests. We used three proteins that are major in blood: bovine serum albumin (BSA) (Aldrich, A9056, St. Louis, U.S.A.), human fibrinogen (HF) (Wako, 061-03693, Osaka, Japan), and immunoglobulin G (IgG) (Aldrich, I4506). They are major proteins in blood. The protein adsorption experiment was performed as follows. The substrates were immersed in a protein solution [phosphate-buffered saline (PBS) (pH 7.4 and 10 mM) of physiological condition containing NaCl (137 mM) and KCl (2.7 mM), and protein concentration 0.5 mg/mL], then rinsed with PBS buffer and deionized water. We characterized the amount of adsorbed protein by XPS, and its dependence of the amount on ρ was discussed with the peak area ratio of $\text{N}_{1s}/\text{Au}_{4f}$.

Platelet Adhesion Tests. Human blood was drawn from healthy volunteers and mixed with a 1/9 volume of acid citrate dextrose (ACD). Platelet-rich plasma (PRP) and platelet-poor plasma (PPP) were obtained by centrifugation of the blood at 1200 rpm for 5 min and at 3000 rpm for 10 min, respectively. Plasma containing 1×10^6 platelets/mL of platelet was prepared by mixing PRP with PPP. The platelet concentration was determined with a cell-counting hematocytometer (Neubauer chamber). Then, 200 μL of the plasma was placed on the SAMs and incubated for 60 min at 37 °C. After the SAMs were washed three times with PBS buffer, they were immersed in 1% glutaraldehyde in PBS for 60 min at 37 °C to fix the platelets adhered on the SAMs. The SAMs were washed three times with PBS, washed with pure water, and then immersed in ethanol to remove the water. We found that this washing procedure did not affect the shapes of platelet cells after their initial adhesion onto solid substrates.²⁰ The samples were sputter-coated with gold (thickness is approximately 2 nm) by prior to observation with a scanning electron microscope (S-4800, Hitachi, Tokyo, Japan).

We acquired at least five scanning electron microscopy (SEM) images (30 $\mu\text{m} \times 40 \mu\text{m}$) at different positions with same ρ . By counting the number of platelets in the images, the average densities of the platelets were calculated ($n = 5$).

AFM Observation of Proteins on the SAMs. AFM observation of adsorbed proteins was performed by ac mode imaging (MFP-3D, Oxford Instruments, U.K.) with a Si cantilever (OMCL-AC160TS, Olympus, Tokyo). For the AFM imaging of the proteins, the substrates after the adsorption test of the proteins were introduced into the liquid cell without drying.

Surface Force Measurements. All force curve measurements were performed with a commercial AFM system equipped with a liquid cell (MFP-3D, Oxford Instruments, U.K.) the same as our previous works.^{14,21} A silica bead (diameter 4 μm , Polysciences, Warrington, PA) was glued at the end of the V-shaped tipless cantilever made of Si_3N_4 (NP-O10, Veeco; the nominal spring constant is 0.06 N/m). The diameter of the bead was calibrated with its optical microscope image. Then, the probe was coated with Ti (thickness 2 nm, adhesion promoter) and Au (thickness 20 nm). The nominal spring constant of the cantilevers was 0.06 N/m. The spring constants were determined by monitoring the thermal fluctuation of the levers. The velocity of the probe approaching to the surface was fixed at 200 nm/s. For the conversion of the deflection of the cantilever to the probe–surface separation, we simply defined a separation of zero as where the linearity in the constant compliance region started in the force–displacement curve. The root mean square (rms) roughness of the Au(111) substrate and Au-coated colloid probes was 0.3 and 0.6 nm, respectively. In this work, the force is expressed based on the Derjaguin approximation (force/radius).

The SAMs for the surface force measurements did not have a chemical gradient. On the basis of the relation between the composition of the thiols and the time for the molecular exchange, we fabricated the SAMs on the Au(111)/mica substrates and Au-coated probes simply by the immersion of the initial monolayer to the

second thiol solution with different reaction times. After the surface force measurements, we characterized exact compositions of the SAMs on the Au(111) substrates by XPS.

Flow of Experiments. The flow of a whole experiment except for the surface force measurements was as follows. First, the fabricated substrate was cut into two or three pieces along the composition gradient. One of them was used for the XPS measurement to evaluate the mixing ratio (about 30 points for one substrate along with the gradient). The other pieces were used for STM, protein adsorption, and platelet adhesion experiments.

RESULTS AND DISCUSSION

STM Observation. In the pure C6-SAM ($\rho = 0$), we observed a $c(4 \times 2)R30^\circ$ structure, which is a typical structure of *n*-alkanethiolates adsorbed on Au(111) surfaces (Figure 1a).^{22,23} At $0 < \rho < 0.3$, the OEG thiolate molecules were

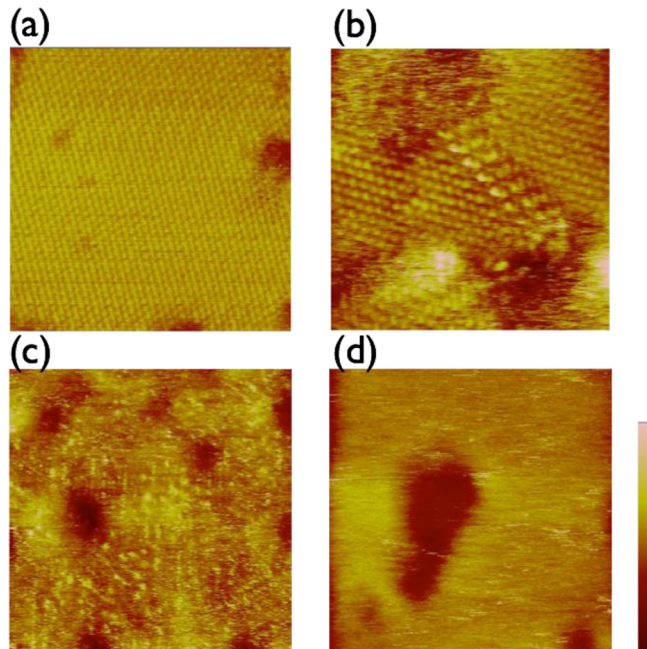


Figure 1. STM images of the mixed SAMs at different ρ : (a) $\rho = 0$ (pure C6-SAM) (image size $20 \text{ nm} \times 20 \text{ nm}$, height 0.5 nm); (b) $\rho = 0.13$ (image size $15 \text{ nm} \times 15 \text{ nm}$, height 0.4 nm); (c) $\rho = 0.40$ (image size $30 \text{ nm} \times 30 \text{ nm}$, height 0.4 nm); (d) $\rho = 1.0$ (pure OEG-SAM) (image size $30 \text{ nm} \times 30 \text{ nm}$, height 0.8 nm).

recognized as brighter spots, since the molecular length of the OEG thiolate is longer than that of the C6 thiolate (the difference is 1.66 nm in all-trans conformation). These two thiolates formed phase-separated domains of OEG and C6 (Figure 1b); the domains of OEG ranging from 1 to 20 nm in size were observed. The formation of the OEG domains was often found at the domain boundaries of the C6-SAM, indicating that the reactivity (exchangeability of the molecules) at the domain boundaries is higher than that in the middle of the domains.²⁴ At $\rho > 0.4$, the crystalline structures of the C6-SAM were hardly observed, and the OEG moieties covered the surface (Figure 1c). As ρ increases further, the STM images lost the clear spots of the OEG chains and became blurred. At $\rho > 0.8$, the phase-separated structures of the SAM completely disappeared because of the flexible OEG moieties fully covering the surface.

Our previous XPS measurements revealed the packing density of OEG thiol is 86% with respect to that of C6-

SAM.¹⁴ As discussed above, C6 and OEG thiolates exist in each phase-separated domain. It is therefore able to estimate the exact ratio of these two entities.

Water Contact Angles. At $\rho < 0.4$, the static water contact angle (WCA) decreased rapidly with an increase of ρ , and the decrease in WCA became insignificant at $\rho > 0.5$. As seen clearly in Figure 2, the trend of WCA as a function of ρ

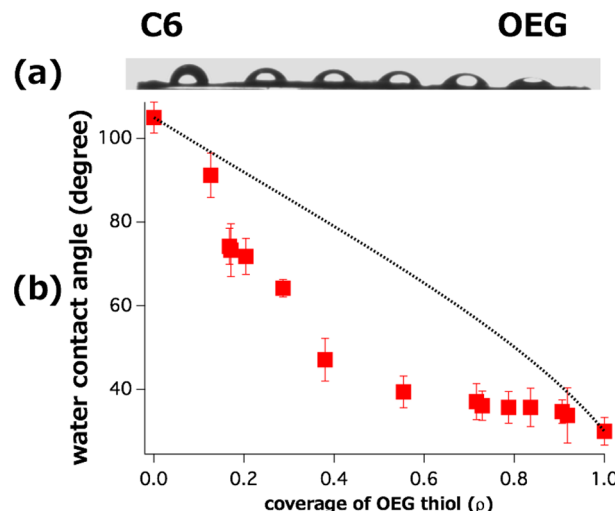


Figure 2. (a) Water droplets ($5 \mu\text{L}$) along the composition gradient of C6 and OEG thiols. (b) Static water contact angles (WCA) measured with droplets of $0.2 \mu\text{L}$ (square dots) plotted as a function of ρ and theoretically predicted WCA (dotted line) based on Cassie's law. (Original WCA data was published in ref 11 and reassembled for discussion.)

deviated from that predicted based on Cassie's law, in which the linear sum of the wetting free energies was simply considered.²⁵ From the STM observation, the surface was almost covered by the OEG chains and at $\rho > 0.5$. Therefore, the lateral density of hydrogen-bonding sites accessible by water molecules did not significantly change, even when the density of the OEG chain increased at $\rho > 0.5$, resulting in a discrepancy between the experimental and theoretically predicted WCAs.

Protein Adsorption. We found that the OEG-SAM exhibited excellent protein resistance, whereas the C6-SAM adsorbed all the proteins used in this work.^{13,14} Both the C6- and OEG-SAMs can be considered as neutral surfaces in the PBS buffer with a physiological condition, in which the Debye screening length is 0.7 nm. Therefore, hydrophobic interaction between the proteins and the hydrophobic C6-SAM is a major driving force for the protein adsorption. Along with the increase of ρ , the amount of the adsorbed proteins decreased monotonically (Figure 3). In addition, we found the thresholds of ρ above which the protein did not adsorb. The trends of the decreases in the amount of adsorbed proteins and the thresholds depended on the kinds of proteins. The decrease as a function of ρ was sharper and the threshold is lower in the case of fibrinogen. In contrast, the decrease was milder, and ρ for the thresholds was higher, in the cases of IgG and BSA.

Previous experimental and theoretical works suggested that local hydrophobic interaction between small hydrophobic domains ($< 1 \text{ nm}$) of surfaces and proteins can be a driving force for the adsorption of the proteins, even though the total area of hydrophilic domains dominated that of hydrophobic domains.^{26–28} Although most of the area is covered by OEG

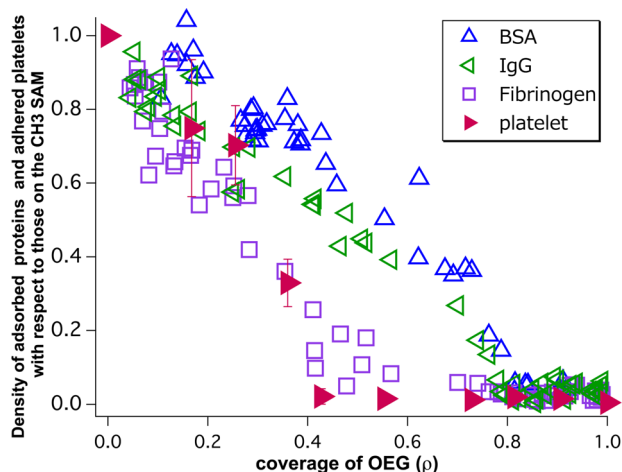


Figure 3. Intensity ratio of N_{1s}/Au_{4f} originated from the adsorbed proteins (original data was published in ref 11 and reorganized for discussion) and density of adhered platelets with respect to those on the C6-SAM as a function of ρ .

chains at $\rho > 0.5$ as observed by STM, very small hydrophobic domains formed via the phase separation of the thiols (Figure 1) still exist. We expect that these “hydrophobic pockets” are adsorption sites for the proteins. Naturally it is expected that a larger area or higher density of adsorption sites is necessary for the adsorption of larger-size proteins. Therefore, we conclude that fibrinogen, whose size is much larger than those of BSA and IgG (Table 1), exhibited a lower threshold of ρ .

Next, we discuss the structure of films composed of the adsorbed proteins and their conformational changes after adsorption. Our AFM measurements revealed that the coverage of fibrinogen at $\rho = 0.4$ is 85% (Figure 4a). The intensity of N_{1s} (not N_{1s}/Au_{4f}) at $\rho = 0.4$ in the XP spectrum was about twice larger than that at $\rho = 0$. Therefore, we concluded that the adsorbed fibrinogen molecules formed at least multilayers at $\rho = 0$. The AFM images showed a clear difference in the morphology of the adsorbed fibrinogen molecules. At $\rho = 0.4$, the molecules formed round-shaped islands (Figure 4a), whereas the molecules formed a flatter structure with smaller bumps at $\rho = 0$ (Figure 4b). We previously analyzed the viscoelasticity of the adsorbed fibrinogen analyzed by quartz crystal microbalance (QCM) with a energy dissipation technique and reported that the conformational change in the fibrinogen on *n*-alkanethiol SAMs was significant than that on the OEG-SAM,¹⁴ in good agreement with the results of AFM observation. Taken together, we concluded that the fibrinogen molecules formed a multilayered structure accompanied by their conformational changes, whereas the coverage of the fibrinogen molecules was less than a monolayer and the molecules maintained relatively native-like states at $\rho = 0.4$.

By judging from the QCM (Table 1), XPS (Figure 3), and AFM observation, the formation of multilayers is not significant in the cases of BSA and IgG. We expect that the denaturation of

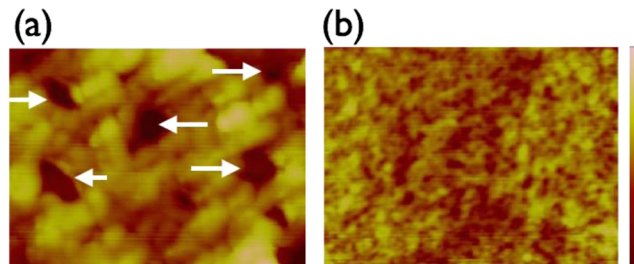


Figure 4. AFM images of fibrinogen adsorbed on the mixed SAM measured in PBS buffer solution: (a) $\rho = 0.4$ (image size 500 nm × 375 nm, height 30 nm). The vacancy of fibrinogen is indicated by the arrows. (b) $\rho = 0$ (pure C6-SAM) (image size 500 nm × 375 nm, height 30 nm). AFM images for IgG and BSA are presented in Supporting Information.

the fibrinogen promoted the formation of multilayers, since hydrophobic residues hidden in the native proteins are exposed to the outside in a denatured state and provide the adsorption site for fibrinogen molecules in the second layer. As summarized in Table 1, the conformational stability of fibrinogen is lower than those of BSA and IgG. We anticipate that the large difference in amounts of adsorbed proteins originates in their conformational stability (Table 1).²⁹

The important finding here is that the amount of the adsorbed proteins cannot be estimated from the WCA, in particular at $0.5 < \rho < 1$. Therefore, it is easily concluded that macroscopic wettability cannot explain the protein resistance and predict the amount of the adsorbed proteins.

Platelet Adhesion. The density of adhered platelets as a function of ρ is displayed in Figure 3, and representative SEM images are presented in Figure 5. When ρ is higher than 0.4, the

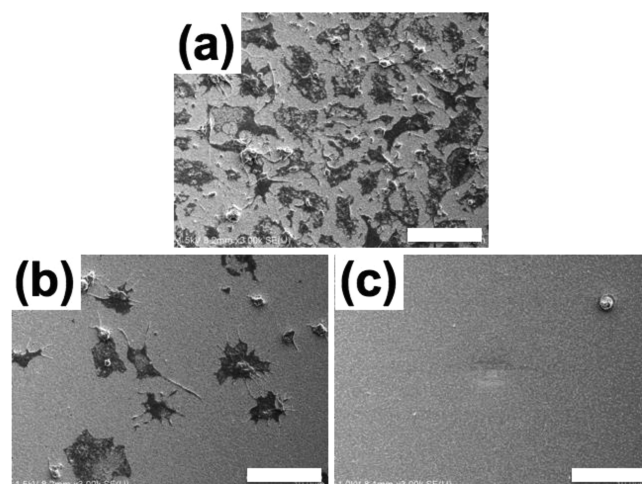


Figure 5. Scanning electron microscope images of platelets adhered on the SAM: (a) $\rho = 0$, (b) $\rho = 0.4$, and (c) $\rho = 1.0$. All scale bars are 10 μm .

Table 1. Structural Properties of Proteins Based on the Information from an Online Protein Data Bank, Amount of the Proteins Adsorbed on the C6-SAM by XPS and QCM (Ref 34), and Thermal Stability of the Proteins (Ref 29)

protein	mol wt (kDa)	dimension (nm)	N_{1s}/Au_{4f}	QCM ($\mu\text{g}/\text{cm}^2$)	denaturation temp (°C)
BSA	69	14 × 4 × 4	0.11 ± 0.01	0.11 ± 0.017	63
IgG	170	24 × 4.4 × 4.4	0.34 ± 0.02	0.11 ± 0.021	64
fibrinogen	340	47 × 5.0 × 5.05	0.50 ± 0.01	0.60 ± 0.22	45

surfaces almost completely repelled platelets. Platelets did not adhere to the substrates in the region of ρ at which fibrinogen did not adsorb ($0.6 < \rho < 1$). Therefore, the resistance to the adsorption of fibrinogen can be used as a criterion for the platelet resistance when the fibrinogen is adsorbed under equivalent solution conditions. This is in good agreement with the report by Tsai et al. in which the suppression of the adsorption of fibrinogen is necessary for platelet resistance.³⁰

Interestingly, although the proteins already adsorbed on the substrate, the surface is still platelet-resistant at $\rho = 0.4$. As discussed before, fibrinogen molecules covered 85% of the total area of the surface at $\rho = 0.4$ with a native-like structure, whereas the adsorbed fibrinogen molecules are denatured at $\rho = 0$ (pure C6-SAM). In the actual platelet adhesion tests, competitive adsorption of various proteins takes place. In this process, proteins with larger molecular weight preferentially adsorb onto the substrate by replacing proteins with smaller molecular weights (so-called "Vroman effect"). Thus, far, several reports have suggested that fibrinogen replaces other plasma proteins during the competitive adsorption.^{31–33} Combining our results and previous findings, we conclude that the conformational change of fibrinogen is a major factor in determining the adhesion of platelets in our system. This finding agrees well with previous reports, in which it was concluded that the denaturation of fibrinogen significantly promotes the platelet adhesion.^{5,6,31} Currently, we are working to identify the adsorbed proteins rigorously by matrix-assisted laser desorption ionization time-of-flight (MALDI-TOF) mass spectrometry to gain deeper insight into the correlation between the composition of the extracellular matrix formed on the SAMs and platelet compatibility.

Surface Force Measurements. We previously performed the systematic analysis of surface force measurements with various combinations of SAMs formed on the probe and substrate.¹⁴ On the basis of the results, we reported that the repulsive interaction at a range of 4–6 nm was induced by the interfacial water in the vicinity of the OEG-SAM (EG3-OH). The interfacial water behaves differently from bulk water and acts as a physical barrier against protein adsorption and platelet adhesion.¹⁴ At $\rho > 0.9$, the water-induced repulsion arose from the separation of 4 nm (Figure 6). At $\rho \leq 0.9$, the repulsive force was weaker than that at $\rho > 0.9$, and the force was

attractive at $\rho = 0.5$. For the pure C6-SAM ($\rho = 0$), strong hydrophobic attraction was dominant (jump-in of the probe to the substrate was observed).

If local hydrophobic domains do not affect the structured interfacial water near the OEG-SAM, the strength of the repulsive force changes while keeping the same distance dependence. However, we found that both the strength and range decreased along with the decrease of ρ . We therefore concluded that the local hydrophobic domains proximate to the OEG domains affected the structured interfacial water in the vicinity of the OEG-SAM. Similar findings were confirmed in our previous report, in which the structuring of the interfacial water near the OEG-SAMs was strongly perturbed by approaching a hydrophobic surface.¹⁴

At $\rho > 0.9$, the small hydrophobic C6 domains are completely covered with OEG chains and the structured interfacial water, resulting in the rejection of adsorption of proteins. By contrast, at $\rho < 0.9$, the interfacial water was perturbed by the hydrophobic C6 domains and the domains worked as adsorption sites for the proteins. Therefore, the surface allowed the adsorption of proteins at $\rho < 0.9$.

Our results also showed that the strength and range of the water-induced repulsion had a clear correlation with protein resistance. On the basis of these results, we concluded that it is important to investigate the behavior of interfacial water to understand the biocompatibility of the surface, which cannot be predicted it only from macroscopic wettabilities.

CONCLUSION

We investigated the correlation among surface structures, water contact angles, protein adsorption, and blood compatibility and interfacial behavior of water molecules using SAMs with a chemical gradient. The results showed that protein adsorption is governed both by sizes of proteins and hydrophobic domains of the substrate. Furthermore, we found a clear correlation between the adsorption of fibrinogen and the adhesion of platelets. Therefore, the resistance to the adsorption of fibrinogen can be used as a criterion for the platelet resistance when the fibrinogen is adsorbed under equivalent solution conditions. From the surface force measurements, we found that the range (distance) and strength of the water-induced repulsion can be employed as criteria for the protein resistance and antiplatelet adhesion effect.

Finally, we propose that self-assembled monolayers with a chemical gradient will provide a very useful platform for systematic analysis of the interaction of organic surfaces with biomolecules and cells. While useful for fundamental research, we expect that such platforms may also be used to design materials to capture target proteins or cells from complex mixtures.

ASSOCIATED CONTENT

S Supporting Information

More information about XPS characterization of the mixed SAMs (Figure S1) and AFM images of IgG and BSA (Figure S2). The Supporting Information is available free of charge on the ACS Publications website at DOI: 10.1021/acs.langmuir.Sb01216.

AUTHOR INFORMATION

Corresponding Author

*E-mail: hayashi@echem.titech.ac.jp.

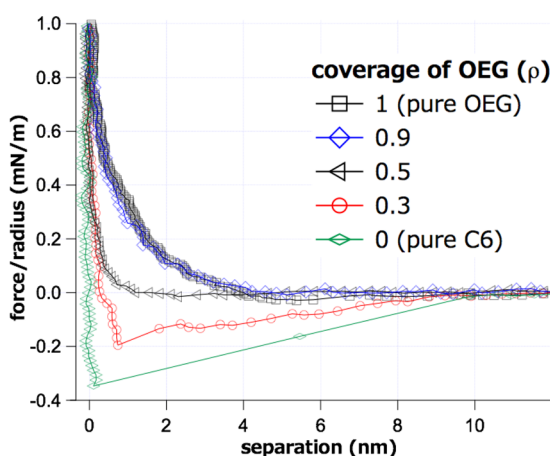


Figure 6. Force–distance curves measured in PBS buffer solution. The identical SAMs were formed on both probe and substrate (symmetric system).

Present Address

[§]Masaru Tanaka, Institute for Materials Chemistry and Engineering, Kyushu University, 744 Motooka Nishi-ku, 819-0395, Japan.

Notes

The authors declare no competing financial interest.

ACKNOWLEDGMENTS

T.H. acknowledges the support of MEXT KAKENHI Grant No. 26282118.

REFERENCES

- (1) Tanaka, M.; Hayashi, T.; Morita, S. The roles of water molecules at the biointerface and application of medical polymers. *Polym. J.* **2013**, *45* (7), 701–710.
- (2) Ratner, B. D. Blood compatibility 2000—foreword. *J. Biomater. Sci., Polym. Ed.* **2000**, *11* (11), 1105–1106.
- (3) Ratner, B. D. Blood compatibility—a perspective. *J. Biomater. Sci., Polym. Ed.* **2000**, *11* (11), 1107–1119.
- (4) Ratner, B. D. The catastrophe revisited: Blood compatibility in the 21st century. *Biomaterials* **2007**, *28* (34), 5144–5147.
- (5) Tanaka, M.; Mochizuki, A.; Motomura, T.; Shimura, K.; Onishi, M.; Okahata, Y. In situ studies on protein adsorption onto a poly(2-methoxyethylacrylate) surface by a quartz crystal microbalance. *Colloids Surf., A* **2001**, *193* (1–3), 145–152.
- (6) Sivaraman, B.; Latour, R. A. The relationship between platelet adhesion on surfaces and the structure versus the amount of adsorbed fibrinogen. *Biomaterials* **2010**, *31* (5), 832–839.
- (7) Sivaraman, B.; Latour, R. A. Time-dependent conformational changes in adsorbed albumin and its effect on platelet adhesion. *Langmuir* **2012**, *28* (5), 2745–2752.
- (8) Mrksich, M.; Whitesides, G. M. Using self-assembled monolayers to understand the interactions of man-made surfaces with proteins and cells. *Annu. Rev. Biophys. Biomol. Struct.* **1996**, *25*, 55–78.
- (9) Love, J. C.; Estroff, L. A.; Kriebel, J. K.; Nuzzo, R. G.; Whitesides, G. M. Self-assembled monolayers of thiolates on metals as a form of nanotechnology. *Chem. Rev.* **2005**, *105* (4), 1103–1169.
- (10) Ulman, A. Formation and structure of self-assembled monolayers. *Chem. Rev.* **1996**, *96* (4), 1533–1554.
- (11) Hayashi, T.; Makiuchi, N.; Hara, M. Self-assembled monolayers with chemical gradients: fabrication and protein adsorption experiments. *Jpn. J. Appl. Phys.* **2009**, *48* (9), 095503–095505.
- (12) Prime, K. L.; Whitesides, G. M. Self-assembled organic monolayers—model systems for studying adsorption of proteins at surfaces. *Science* **1991**, *252* (5009), 1164–1167.
- (13) Prime, K. L.; Whitesides, G. M. Adsorption of proteins onto surfaces containing end-attached oligo(ethylene oxide)—a model system using self-assembled monolayers. *J. Am. Chem. Soc.* **1993**, *115* (23), 10714–10721.
- (14) Hayashi, T.; Tanaka, Y.; Koide, Y.; Tanaka, M.; Hara, M. Mechanism underlying bioinertness of self-assembled monolayers of oligo(ethyleneglycol)-terminated alkanethiols on gold: protein adsorption, platelet adhesion, and surface forces. *Phys. Chem. Chem. Phys.* **2012**, *14* (29), 10196–10206.
- (15) Kraus, T.; Stutz, R.; Balmer, T. E.; Schmid, H.; Malaquin, L.; Spencer, N. D.; Wolf, H. Printing chemical gradients. *Langmuir* **2005**, *21* (17), 7796–7804.
- (16) Ballav, N.; Shaporenko, A.; Krakert, S.; Terfort, A.; Zharnikov, M. Tuning the exchange reaction between a self-assembled monolayer and potential substituents by electron irradiation. *J. Phys. Chem. C* **2007**, *111* (21), 7772–7782.
- (17) Ballav, N.; Shaporenko, A.; Terfort, A.; Zharnikov, M. A flexible approach to the fabrication of chemical gradients. *Adv. Mater.* **2007**, *19* (7), 998–.
- (18) Meyyappan, S.; Shadnam, M. R.; Amirfazli, A. Fabrication of surface energy/chemical gradients using self-assembled monolayer surfaces. *Langmuir* **2008**, *24* (6), 2892–2899.
- (19) Morgenthaler, S.; Lee, S. W.; Zurcher, S.; Spencer, N. D. A simple, reproducible approach to the preparation of surface-chemical gradients. *Langmuir* **2003**, *19* (25), 10459–10462.
- (20) Tanaka, M.; Mochizuki, A. Effect of water structure on blood compatibility—thermal analysis of water in poly(meth)acrylate. *J. Biomed. Mater. Res., Part A* **2004**, *68A* (4), 684–695.
- (21) Hayashi, T.; Tanaka, Y.; Usukura, H.; Hara, M. Behavior of hydroxide ions in vicinity of self-assembled monolayers of alkanethiols on metals. *e-J. Surf. Sci. Nanotechnol.* **2009**, *7*, 601–605.
- (22) Poirier, G. E.; Tarlov, M. J. The C(4 × 2) superlattice of *n*-alkanethiol monolayers self-assembled on Au(111). *Langmuir* **1994**, *10* (9), 2853–2856.
- (23) Hayashi, T.; Kodama, C.; Nozoye, H. Structural evolution of dibutyl disulfide adsorbed on Au(111). *Appl. Surf. Sci.* **2001**, *169*, 100–103.
- (24) Poirier, G. E. Characterization of organosulfur molecular monolayers on Au(111) using scanning tunneling microscopy. *Chem. Rev.* **1997**, *97* (4), 1117–1127.
- (25) Cassie, A. B. D.; Baxter, S. Wettability of porous surfaces. *Trans. Faraday Soc.* **1944**, *40*, 0546–0550.
- (26) Ostuni, E.; Grzybowski, B. A.; Mrksich, M.; Roberts, C. S.; Whitesides, G. M. Adsorption of proteins to hydrophobic sites on mixed self-assembled monolayers. *Langmuir* **2003**, *19* (5), 1861–1872.
- (27) Zuyderhoff, E. M.; Dupont-Gillain, C. C. Nano-organized collagen layers obtained by adsorption on phase-separated polymer thin films. *Langmuir* **2012**, *28* (4), 2007–2014.
- (28) Hung, A.; Mwenifumbo, S.; Mager, M.; Kuna, J. J.; Stellacci, F.; Yarovsky, I.; Stevens, M. M. Ordering surfaces on the nanoscale: implications for protein adsorption. *J. Am. Chem. Soc.* **2011**, *133* (5), 1438–1450.
- (29) van Stokkum, I. H.; Linsdell, H.; Hadden, J. M.; Haris, P. I.; Chapman, D.; Bloemendaal, M. Temperature-induced changes in protein structures studied by Fourier transform infrared spectroscopy and global analysis. *Biochemistry* **1995**, *34* (33), 10508–10518.
- (30) Tsai, W. B.; Grunkemeier, J. M.; Horbett, T. A. Human plasma fibrinogen adsorption and platelet adhesion to polystyrene. *J. Biomed. Mater. Res.* **1999**, *44* (2), 130–139.
- (31) Nonckreman, C. J.; Fleith, S.; Rouxhet, P. G.; Dupont-Gillain, C. C. Competitive adsorption of fibrinogen and albumin and blood platelet adhesion on surfaces modified with nanoparticles and/or PEO. *Colloids Surf., B* **2010**, *77* (2), 139–149.
- (32) Bale, M. D.; Mosher, D. F.; Wolfarht, L.; Sutton, R. C. Competitive adsorption of fibronectin, fibrinogen, immunoglobulin, albumin, and bulk plasma-proteins on polystyrene latex. *J. Colloid Interface Sci.* **1988**, *125* (2), 516–525.
- (33) Pandey, L. M.; Pattanayek, S. K. Properties of competitively adsorbed BSA and fibrinogen from their mixture on mixed and hybrid surfaces. *Appl. Surf. Sci.* **2013**, *264*, 832–837.
- (34) The discrepancy in the amounts of the adsorbed proteins evaluated by XPS and QCM may be due to the difference in rinsing processes. In addition, it can also be the origin of the discrepancy that XPS measures amount of nitrogen and QCM measures water-containing mass on the other hand.